



## Spectroscopic Mapping Ellipsometry of Graphene Grown on 3C SiC

Journal:	<i>2011 MRS Fall Meeting</i>
Manuscript ID:	Draft
Manuscript Type:	Symposium AA
Date Submitted by the Author:	n/a
Complete List of Authors:	Boosalis, Alexander Hofmann, Tino; University of Nebraska - Lincoln, Electrical Engineering Darakchieva, Vanya; Linköping University, Physics Yakimova, Rositza; Linköping University, Physics Tiwald, Tom; J.A.Woollam Co. Inc. Schubert, Mathias; University of Nebraska - Lincoln, Electrical Engineering
Keywords:	dielectric properties, epitaxy, C

SCHOLARONE™  
Manuscripts

## Spectroscopic Mapping Ellipsometry of Graphene Grown on 3C SiC

Alexander Boosalis<sup>1</sup>, Tino Hofmann<sup>1</sup>, Vanya Darakchieva<sup>2</sup>, Rositza Yakimova<sup>2</sup>, Tom Tiwald<sup>3</sup>, and Mathias Schubert<sup>1</sup>

<sup>1</sup>Department of Electrical Engineering and Nebraska Center for Materials and Nanoscience, University of Nebraska – Lincoln, U.S.A.

<sup>2</sup>Department of Physics, Linköping University, Linköping Sweden.

<sup>3</sup>J.A. Woollam Co., Lincoln, Nebraska, U.S.A.

### ABSTRACT

Spectroscopic mapping ellipsometry measurements in the visible spectrum (1.25 to 5.35 eV) are performed to determine the lateral variations of epitaxial graphene properties as grown on 3C SiC. Data taken in the visible spectrum is sensitive to both the Drude absorption of free charge carriers and the characteristic exciton enhanced van Hove singularity at 5 eV. Subsequent analysis with simple oscillator models allows the determination of physical parameters such as free charge carrier scattering time and local graphene thickness with a resolution of approximately 50 microns.

### INTRODUCTION

Recent research has shown graphene to exhibit superior electronic properties to silicon leading to a demand for epitaxial graphene production [1, 2]. Successful deposition of epitaxial graphene onto large scale substrates, perhaps by thermal sublimation of silicon carbide, may offer realization of a new generation of electronic devices. Recently, fabrication of field-effect transistor devices on epitaxial graphene with cut-off frequencies in excess of fifty gigahertz was achieved [3]. In order to harness graphene for commercial production, further development of epitaxial growth processes must continue and a better understanding of the electronic and structural relationships in epitaxial graphene must be reached [4, 5].

In order to better understand the influences of substrate morphology and surface preparation on graphene growth and resulting electronic properties we must investigate the laterally varying dielectric function of epitaxial graphene films. The dielectric function spectra are unique fingerprints of the electronic properties of semiconductor materials, and are suitable for characterization of electronic band structure parameters. Likewise, these functions can be used for monitoring structure-related properties such as strain, as well as for quality control during production.

Theoretical calculations predict a van Hove singularity within the 2-dimensional Brillouin zone along the 6-fold degenerate directions between symmetry points K and K' [6]. This singularity can be associated with the characteristic critical-point feature observed in dielectric function spectra of exfoliated graphene [7, 8], and graphene grown by chemical vapor deposition for photon energies around 5~eV [9]. It is of interest to monitor these critical-point features as a function of position, which may reflect differences in strain and dopant and defect incorporation of the epitaxial graphene layers.

The physical parameter maps reported here are obtained from spectroscopic ellipsometry measurements and subsequent model dielectric function analysis. We employ traditional physical

model lineshape analysis procedures, and provide physical parameters of graphene in the visible spectrum across a large surface area. We suggest systematic ellipsometric investigations of epitaxial graphene to identify the influences of surface morphology and doping- and adsorbent-induced free carrier density variations.

## EXPERIMENT

The sample investigated was formed by thermal sublimation of silicon from a 3C SiC epitaxial layer as grown on the Si face (0001) of a 6H SiC substrate. The sample was stored in normal ambient after growth and not further treated. Mapping ellipsometry measurements were thermally treated 3C sample. An untreated 3C substrate was measured to determine the dielectric response of the silicon carbide without graphene. From these measurements, the dielectric functions of the substrate was obtained. All measurements were performed on a J.A. Woollam M2000 ellipsometer with focusing probes to reduce spot size to 50 microns in diameter. Measurements were performed for photon energies from 1.25 to 5.35 eV, at an angle of incidence of 65 degrees.

Ellipsometry determines the ratio  $\rho$  of the complex-valued Fresnel reflection coefficients  $r_p$  and  $r_s$  for light polarized parallel ( $p$ ) and perpendicular ( $s$ ) to the plane of incidence, respectively, and is commonly presented with parameters  $\Psi$  and  $\Delta$  as in Eqn. 1 [10, 11, 12].

$$\rho = r_p / r_s = \tan(\Psi) e^{i\Delta} \quad (1)$$

A layer model is required for analysis of data from samples with multiple layer constituents. Sample models include a substrate, an interface layer between the substrate and the graphene, and a pure graphene layer. All layers are treated isotropically in our model since ellipsometry has no sensitivity to the out-of-plane polarizability of ultra thin layers [13, 14]. The dielectric functions of all constituents (substrate, transition layer, graphene) are parameterized by model dielectric function (MDF) approaches. The MDF for the substrate must be determined first. Experimental  $\Psi$  and  $\Delta$  spectra obtained from a non-thermally treated 3C SiC substrate were analyzed employing a sum of broadened harmonic oscillator lineshapes. The best-match MDF parameters are omitted here for brevity. The obtained MDF spectra are equivalent to those reported previously for 3C SiC [15]. The best-match MDF parameters for each substrate were then used in the calculation of the best-match MDF parameters for the graphene layers of the thermally treated samples. The graphene MDF is implemented here following Nelson *et al.* by a sum of a Lorentzian and Gaussian broadened harmonic oscillator lineshapes [9]. Included is a Lorentzian oscillator with a characteristic frequency of zero (Drude model) to account for free charge carrier absorption.

The interface layer is formed by carbon atoms that are strongly bonded to the substrate [16]. A linear effective medium approximation (EMA) comprised of the substrate and pure graphene MDFs was used to create a suitable MDF for the transition layer. The only varied parameter during the fitting process that was unique to the transition layer was its constituent percentage ( $X$ ), the thickness was fixed to a value of 0.4 nm as established in literature [17]. The transition layer can then be viewed as an MDF of  $G_X \text{SiC}_{(1-X)}$ . Parameters varied during data analysis include the amplitudes, the critical-point transition energies, and the broadening of each harmonic oscillator, including the Drude scattering time  $\tau_s$ . During data analysis, the thicknesses of the epitaxial graphene layer  $t_G$ , the transition layer constituent percentage  $X$ , and the graphene

MDF parameters are varied until best-match between experimental and model calculated  $\Psi$  and  $\Delta$  is achieved.

## DISCUSSION

Examples of individual  $\Psi$  and  $\Delta$  spectra can be seen in Fig. 1. Data in Fig. 1A were taken from a region with large graphite-like carbon growth, while data in Fig. 1B were taken from a region with graphene growth. In order to match the van Hove singularity around 5 eV, two harmonic oscillators are required. Comparison between Fig. 1A and Fig. 1B reveals a red shift of the lower energy harmonic oscillator, along with an increase in amplitude and a decrease in broadening, displaying a profound difference between graphene and graphite-like carbon spectra.

Fig. 2A shows the graphene thickness parameter  $t_G$  as a function of  $x$  and  $y$  coordinates, utilizing a spline function to render smooth 3D surfaces. We observe that the nominal graphene thickness is 0.4 nm, accepted as the typical thickness of a graphene monolayer [17]. This nominal value is broken by areas of graphite-like carbon growth, most notably around coordinates (-0.11, 0.05) and (0.05, -0.03), which approach thicknesses of 6 nm. These areas of increased graphite-like growth are the result of fissures in the 3C substrate leftover from the polishing process, providing increased crystal dislocations and surface area for rapid graphene growth [18].

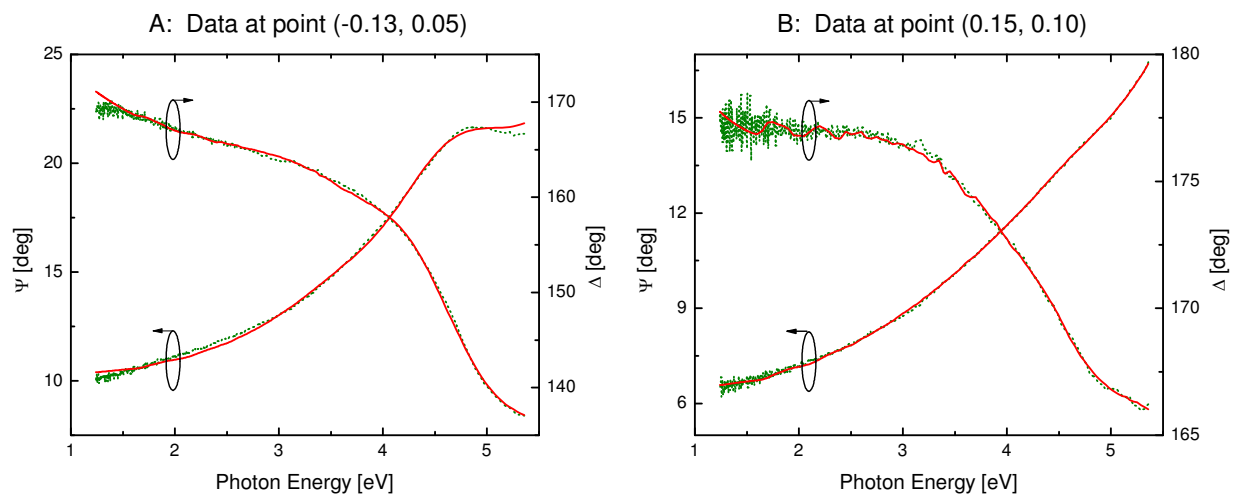


**Figure 1.** A:  $\Psi$  and  $\Delta$  spectra taken at location coordinates (-0.13, 0.05) showing data for a region with thick graphite-like carbon. B:  $\Psi$  and  $\Delta$  spectra taken at location coordinates (-0.15, 0.10) showing a region with graphene. Green dotted lines represent experimental data while solid red lines represent the best match model.

Fig. 2B shows the graphene scattering time parameter  $\tau_s$  as a function of  $x$  and  $y$  coordinates. It is clear that scattering times at the coordinates of increased graphite-like carbon growth display values approaching zero, showing decreased mobility for free charge carriers. Also present in Fig. 2 are several scattering time peaks, the largest of which is located around coordinate (0.09, -0.11). Observing the graphene thickness at this location in Fig. 1, we see that the thickness corresponds to a bilayer of graphene, positioned between two much thicker regions. The heightened scattering time in these areas may then be attributed two possible scenarios.

Perhaps the SiC has been completely etched away beneath the graphene layer, leaving a suspended graphene layer unaffected by substrate material. Alternatively, the thick regions of graphite-like growth could be enforcing non-stratified growth of a graphene monolayer, resulting in higher scattering times.

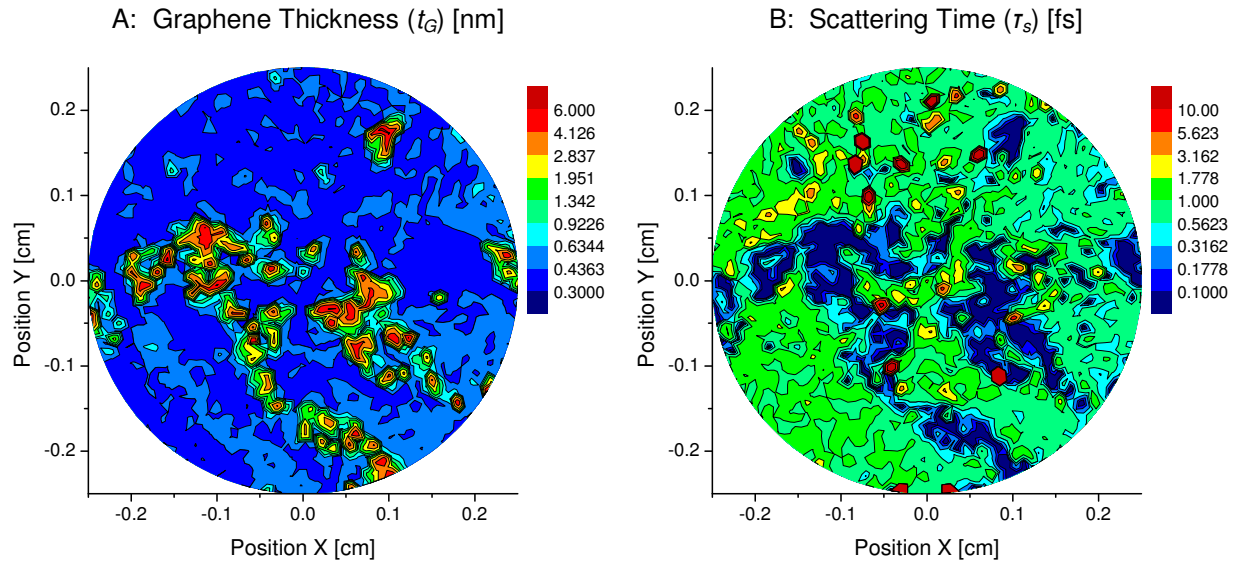


**Figure 2.** False color images of the best match model parameters  $t_G$  (A, in nm) and  $\tau_s$  (B, in femtoseconds) as functions of  $x$  and  $y$  coordinates.

## CONCLUSION

In conclusion, mapping spectroscopic ellipsometry measurements have been performed on epitaxial graphene grown 3C SiC. A two layer system was used to model the resulting data, with a simple harmonic oscillator dielectric response model used for graphene. Maps of best match model parameters including the graphene thickness and scattering time were compared, showing decreased scattering time where thick graphite-like growths were present. The maximum scattering time was found to occur on a graphene monolayer located between two thick graphite-like growths.

## ACKNOWLEDGMENTS

The authors would like to acknowledge financial support from the Army Research Office (W911NF-09-C-0097), the National Science Foundation (MRSEC DMR-0820521, MRI DMR-0922937, DMR-0907475, ECCS-0846329, and EPS-1004094), the University of Nebraska-Lincoln, and the J.A. Woollam Foundation.

## REFERENCES

1. K. Bolotin, K. Sikes, Z. Jiang, M. Klima, G. Fudenberg, J. Hone, P. Kim, and H. Stormer, *Solid State Commun.*, **146**, 351 (2008).

2. J. Dawlaty, S. Shivaraman, M. Chandrashekar, F. Rana, and G. Spencer, *Appl. Phys. Lett.*, **92**, 042116 (2008).
3. Y. Lin, H. Chiu, K. Jenkins, D. Farmer, P. Avouris and A. Valdes-Garcia, *Electron Devic. Lett.*, **31**, 68 (2010).
4. D. Gaskill, G. Jernigan, P. Campbell, J. Tedesco, J. Culbertson, B. VanMil, R. Myers-Ward, C. Eddy, J. Moon, D. Curtis, M. Hu, D. Wong, C. McGuire, J. Robinson, M. Fanton, J. Stitt, D. Snyder, X. Weng, and E. Frantz, *ECS Trans.*, **19**, 117 (2009).
5. P. First, W. Heer, T. Seyller, C. Berger, J. Stroscio and J. Moon, *MRS Bull.*, **35**, 296 (2010).
6. T. Stauber, N. Peres, A. Geim, *Phys. Rev. B.*, **78**, (2008).
7. V. Kravets, A. Grigorenko, R. Nair, P. Blake, S. Anissimova, K. Novoselov, and A. Geim, *Phys. Rev. B.*, **81**, (2010).
8. J. Weber, V. Calado, and M. Sanden, *Appl. Phys. Lett.*, **97**, 091904 (2010).
9. F. Nelson, V. Kamineni, T. Zhang, E. Comfort, J. Lee, and A. Diebold, *Appl. Phys. Lett.*, **97**, 253110 (2010).
10. R. Azzam and N. Bashara, "Ellipsometry and Polarized Light," (North-Holland Publ. Co., 1984).
11. M. Schubert, "Infrared Ellipsometry on Semiconductor Layer Structures: Phonons, Plasmons, and Polaritons," (Springer, 2004).
12. H. Fujiwara, "Spectroscopic Ellipsometry," (John Wiley & Sons, 2007).
13. H. Thompkins and E. Irene, "Handbook of Ellipsometry," (William Andrew Publishing, 2004).
14. M. Schubert, B. Rheinlander, J. Woollam, B. Johs, and C. Herzinger, *J. Opt. Soc. Am. A.*, **13**, 875 (1996).
15. S. Logothetidis and J. Petalas, *J. Appl. Phys.*, **80**, 1768 (1996).
16. J. Hass, F. Varchon, J. Millan-Otoya, M. Sprinkle, N. Sharma, W. Heer, C. Berger, P. First, L. Magaud, and E. Conrad, *Phys. Rev. Lett.*, **100**, 125504 (2008).
17. F. Varchon, R. Feng, J. Hass, X. Li, B. Nguyen, C. Naud, P. Mallet, J. Veuillen, C. Berger, E. Conrad, and L. Magaud, *Phys. Rev. Lett.*, **99**, 126805 (2007).
18. J. Hite, M. Twigg, J. Tedesco, A. Friedman, R. Myers-Ward, C. Eddy, and D. Gaskill, *Nano Lett.*, **11**, 1190 (2011).